New Tasseled Cap Classification Technique using Landsat-8 OLI Image Bands

S.M. Ali[1], S.S. Salman[2*]

[1]Department of Remote Sensing, College of Science University of Baghdad, Baghdad, Iraq
[2]Department of Clinical Laboratory Science College of Pharmacy, University of Baghdad, Baghdad, Iraq

Abstract

The tasseled cap transformation (TCT) is a useful tool for compressing spectral data into a few bands associated with physical scene characteristics with minimal information loss. TCT was originally evolved from the Landsat multi-spectral scanner (MSS) launched in 1972 and is widely adapted to modern sensors. In this study, we derived the TCT coefficients for operational land imager (OLI) sensor on-board Landsat-8 acquired at 28 Sep.2013. A newly classification method is presented; the method is based on dividing the scatterplot between the Greenness and the Brightness of TCT into regions corresponding to their reflectance values. The results from this paper suggest that the TCT coefficient derived from the OLI bands at September is the most appropriate for harness these features to calculate the acreage of rice and compare them with the declared areas by the Iraqi Ministry of Agriculture to make sure of their accuracy.

Keywords: Tasseled Cap Transformation, Greenness coefficient, Brightness coefficient

تقنية جديدة للتصنيف بالاعتماد على تحويل الغطاء الخضري

صالح مهدي علي[1]، سليمة سلطان سلمان[2*]

[1]قسم التحسس النائي ، كلية العلوم ، جامعة بغداد، بغداد، العراق

[2]فرع العلوم المختبرية ، كلية الصيدلة ، جامعة بغداد، بغداد، العراق

الخلاصة

تعتبر تحويلة الغطاء الخضري (TCT) أحد الأدوات المفيدة لضغط البيانات الطيفية إلى عدد من الحزم المرتبطة بخصائص المشهد االفيزيائية مع فقدان الحد الأدنى من المعلومات. تطورت تحويلة الغطاء الخضري أصلا من صور الماسح الضوئي للاندسات متعدد الأطياف (MSS) الذي أطلق في عام 1972 والذي تم تطويره ليتلائم مع نطاق واسع من صور أجهزة الاستشعار الحديثة. في هذه الدراسة، تم تسخير معاملات الغطاء الخضري للتعامل مع صور الحزم الناتجة من القمر لاندسات−8 لتصوير الأرض (OLI) الملتقطة في شهر أيلول في عام 2013. تم في هذا البحث تقديم طريقة جديدة لتصنيف مناطق الصور الفضائية. تعتمد هذه الطريقة على تقسيم مخطط التبعثر بين حزم الإخضرار والسطوع للغطاء الخضري إلى مناطق إعتماداً على قيم إنعكاسيتها. تشير نتائج هذه الدراسة إلى أن معاملات الغطاء الخضري المستمدة من صورة شهر إيلول هي الأنسب لتسخير هذه الميزات لحساب المساحات المزروعة بالرز ومقارنتها مع المساحات التي أعلنتها وزارة الزراعة العراقية للتأكد من دقتها.

الكلمات المفتاحية : تحويل الغطاء الخضري ، معامل الخضري ، معامل السطوع .

_____

*Email: smalitokmachi@scbaghdad.edu.iq

Introduction

Presently too many satellites and remote sensing data have been used for monitoring Landcover and Landuse components of the Earth's surface. Among all, series of Landsat have been the most widely used remote sensing satellite, which have collected a historical archive in earth observation in the past four decades and made significant contributions to the agriculture and water management, global ecosystem, environmental change and disaster monitoring. Landsat-8, launched on February 11, 2013, is the 8th of the series of Landsat satellites which makes the continuity of Landsat earth observation mission possible and provides the long time-series availability of Landsat images for regional application researches [1]. The TCT is the conversion of the satellite bands into a set of weighted sums of separate channel readings. One of these weighted sums measures roughly the *brightness* of each pixel in the scene, another composite represents the degree of *greenness* of the pixels, and another might represent the degree of *yellowness* of vegetation or perhaps the *wetness* of the soil [2].

For example, Kauth and Thomas [2] represent a plot for a real wheat field by combining the soil reflectance and green stuff and then adding yellow stuff. The plot as shown in Figure-1 was resembled a cap shape.
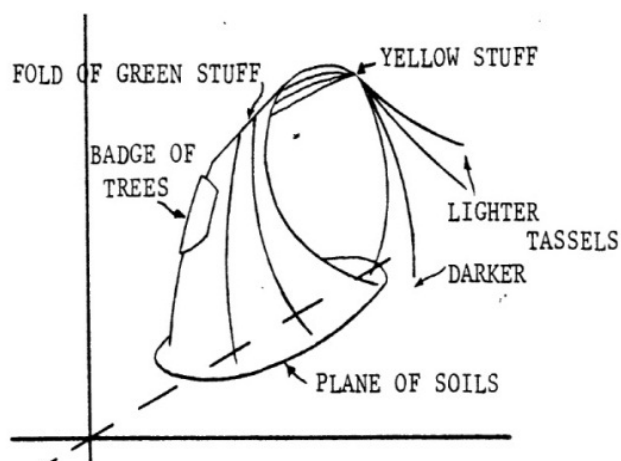

Figure 1- Plot of Tasseled Cap for real wheat field [3]

For Landsat MSS images, the TCT weights were introduced by Kauth and Thomas [3] used to determine the TCT components. However, a change to a new satellite sensor needs alternative weights for the TCT. For example, The TCT weights for Landsat 4-5 Thematic Mapper (TM) and Landsat 7 Enhanced Thematic Mapper Plus (ETM+) were introduced by Muhammad, etc. [1] are used to compute the TCT components. Because the Landsat-8 sensors capture reflected solar energy of 16-bits data (range from $0 \rightarrow 65536$), a specific weights have been developed by [1] to compute the TCT components. Other weights have been developed for other satellite sensors, for instance for *JERS-1 OPS* image sensor see [3], for ASTER image sensor see [4], for SPOT-5 image sensors see [5], for IKONOS image sensors see [6], for QUICKBIRD-2 image sensors see [7]. In our present research, because the OLI image bands will be corrected to the Top of Atmospheric (TOA) reflectance, their bands reflectance values will have the range $(0.005387 \rightarrow 1.346932)$, accordingly the TCT weights that are used to compute the TCT components of ETM+ images will be adopted to compute the OLI TCT components.

The Study Area

The investigation has been performed on parts of Al-Najaf and Al-Qadisiya provinces in the middle-south of Iraq, at $32.216° \rightarrow 31.550°$N latitude, and $44.161° \rightarrow 44.724°$E longitude, as shown in Figure-2. It has been selected because they represent the central area for rice production in Iraq. It is a fertile mudslides land area, about 30km south of Najaf province, 230 km southwest of the Baghdad (capital of Iraq). A river (called Al-Hidia) of length 25km, which is part of the Euphrates River, passes through them. The study area is surrounded by rice plantations and palm groves.
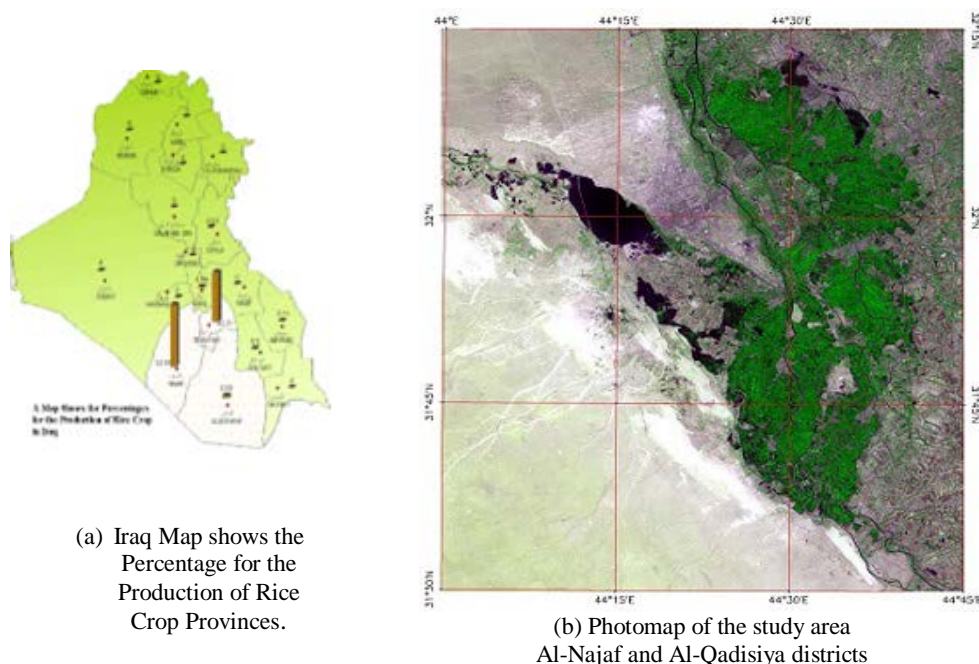
(a) Iraq Map shows the Percentage for the Production of Rice Crop Provinces.

(b) Photomap of the study area
Al-Najaf and Al-Qadisiya districts

Figure 2- (a) Administrative map of Iraq country shows the percentages for the production of rice crop, and (b) a photomap of the study area

Radiometric Correction of Images

The OLI instrument consists of 9-spectral channels ranging from visible to shortwave infrared wavelengths. When compared to ETM+, OLI has two additional channels: the deep blue band at 0.443 μm for coastal and aerosol measurements and the cirrus band at 1.375 μm for cirrus cloud detection. The OLI is a pushbroom sensor instead of the whiskbroom sensors used on earlier Landsat satellites (1–7). The spatial resolution and swath width of the OLI are comparable to the ETM+. The Focal Plane Array (FPA) consists of 14 Focal Plane Modules (FPMs) made up of detectors and spectral filters for each band. Silicon detectors are used for visible to near infrared (NIR) bands with Mercury Cadmium Telluride detectors for the SWIR bands [1-3]. There are about 7000 across-track detectors per spectral channel except for the panchromatic band, which has nearly 14,000 detectors. OLI has multiple onboard radiometric sources, namely two spectral on solar diffusers and three pairs of lamps. OLI data are quantized to 12 bits; this is higher than ETM+ and Thematic Mapper (TM) where they were quantized to 8 bits. The Landsat sensors capture reflected solar energy, convert them to radiance, and then rescale those data into 16-bits Digital Number DN (range between $0 \rightarrow 65536$). The OLI band data can also be converted to TOA planetary reflectance using reflectance rescaling coefficients provided in the product *metadata* file (MTL file), provided by. The following equation is used to calibrate the OLI image "DN" values to TOA reflectance:

$$\rho_\lambda = \frac{M_\rho Q_{cal} + A_\rho}{Cos(\theta_{sz})} \tag{1}$$

Where: ρ_λ = TOA planetary reflectance, M_ρ = Bandspecific multiplicative, A_ρ = Bandspecific additive, Q_{cal} = Quantized and calibrated standard product pixel values (DN), θ_{SZ} = Local solar zenith angle; θ_{SZ} = 90° - θ_{SE} where θ_{SE} = Local sun elevation angle.

Figure-3 shows the original OLI bands combination and their histograms before and after the TOA calibration process.
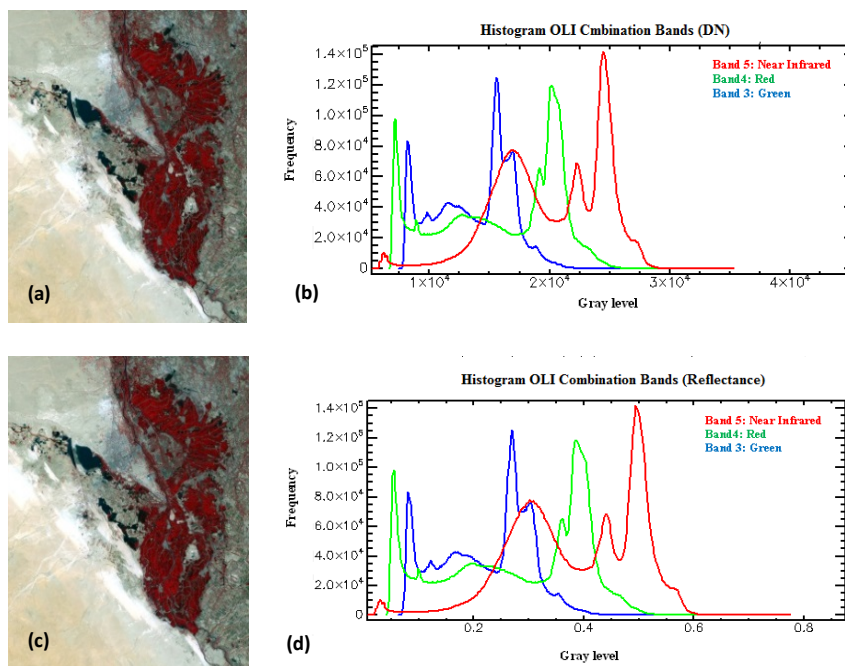
Figure 3- (a) Reflectance OLI colored image acquired at 2013-9-28, (b) its histograms, (c)TOA calibrated OLI colored image, and (d) its histograms.

Tasseled Cap Transformation (TCT)

As mentioned above, the TCT of the TOA calibrated bands of OLI is computed in similar way to those used for Landsat-7 (ETM+) images. Only the *Brightness*, *Greenness*, and *Wetness* components are determined using the TCT weights shown in Table-1.

Table 1- Weights of TCT for OLI calibrated bands images [1]

Components	Band-2 Blue	Band-3 Green	Band-4 Red	Band-5 NIR	Band-6 SWINR-1	Band-7 SWINR-2
Brightness	0.3037	0.2793	0.4743	0.5585	0.5082	0.1863
Greenness	-0.2848	-0.2435	-0.5436	0.7243	0.0840	-0.1800
Wetness	0.1509	0.1973	0.3279	0.3406	-0.7112	-0.4572

The calculated components of calibrated OLI, acquired at Sept.2013 are shown in Figure-4.
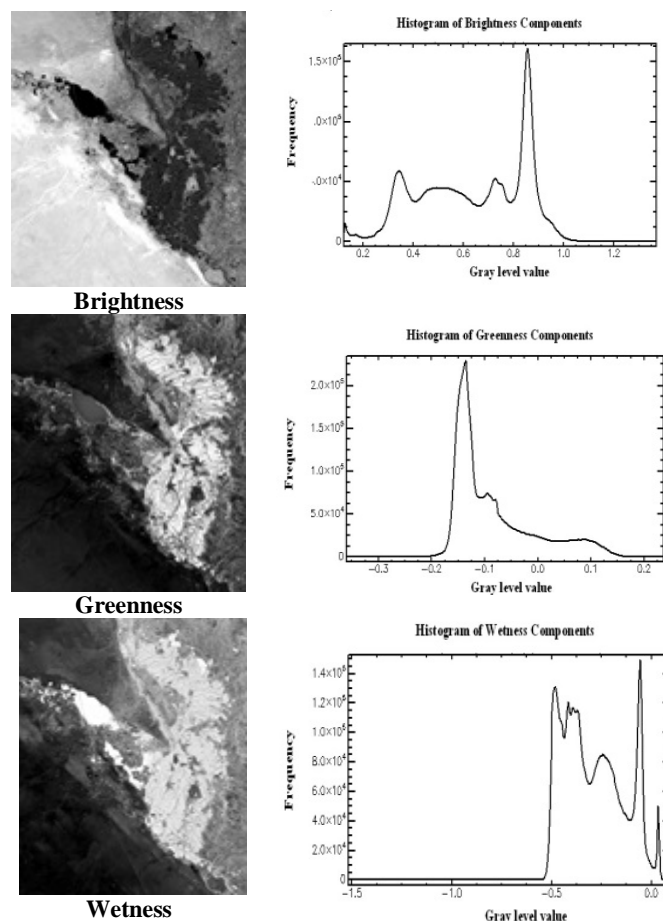
Figure 4- The TCT components of the calibrated ETM+ bands and their histograms.

TCT Scatter Plot Classification

In our previous paper [9], we have utilized the scatterplot between the red and near-infrared bands of Landsat-7 (ETM+) to classify the Landcover components of the study area. In follow-up papers we have used that scattering classification technique to validate the planted areas with rice and compare them with the true planted areas obtained from the Iraqi Ministry of Agriculture publications, see [9,10]. In this paper, a new automatic scatterplot classification method will be introduced based on utilizing the TCT components of the calibrated bands of the Landsat-8 (OLI). Figure-5 illustrates the scatterplot of the original calibrated red and near-infrared OLI bands and the scatterplot of the brightness and greenness components of the TCT.
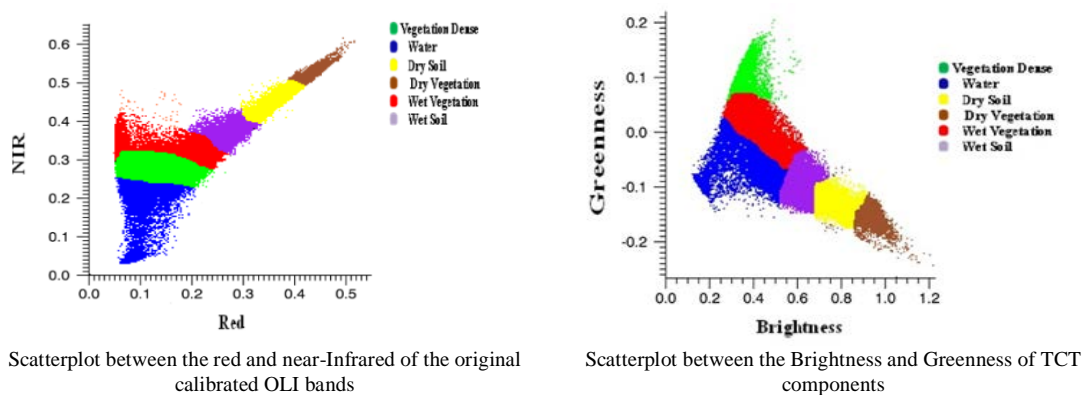
Scatterplot between the red and near-Infrared of the original calibrated OLI bands

Scatterplot between the Brightness and Greenness of TCT components

Figure 5- Scatterplots between the original OLI bands and the TCT components showing the locations of each Landcover classes (i.e. Dense Vegetation, water, dry soil, dry vegetation, wet vegetation, and wet soil)

Scatterplot between the Brightness andWetness of TCT components

Scatterplot between the Wetness and Greenness of TCT components

Figure 5- Scatterplots between the original OLI bands and the TCT components showing the locations of each Landcover classes (i.e. Dense Vegetation, water, dry soil, dry vegetation, wet vegetation, and wet soil)
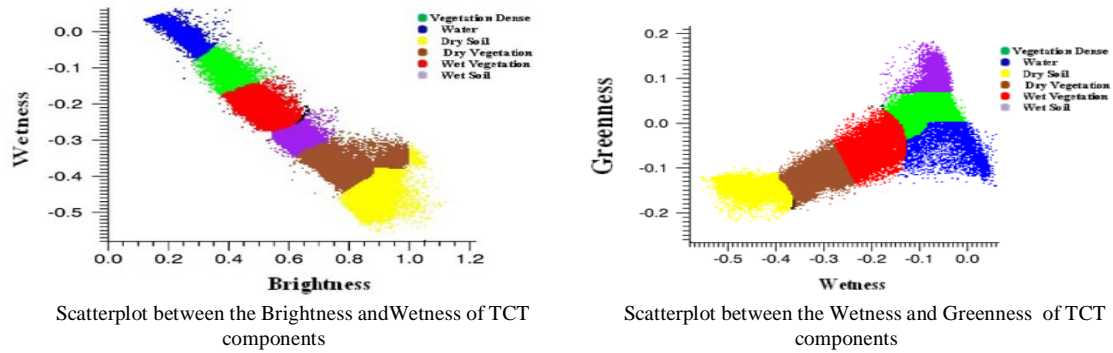
Because of the similarity in the behavioral of the brightness and greenness with that between the red and near-infrared bands, thus a new automatic classification method is introduced in this paper similarly to that presented in [9]. The procedures involved in this classification method are illustrated in the block-diagram of Figure-6.

Input OLI Bands
Table-1

Compute the TCT Components
Brightness (Br) and Greenness (Gr)

Find Coordinates of Soil Line

$$Soil(x, y) = \sqrt{[Br(x, y)]^2 + [Gr(x, y)]^2}$$

Find Soil Line Extremist Points;
Min{Soil(x, y)} and Max{Soil(x, y)}

Find Soil Line points using 1ˢᵗ order Polynomial curve fitting

$$\mathbf{y = mx + b}$$

"b" represents the intersection with *"Greenness"* axis, and

$$m = \frac{Max(Gr) - Min(Gr)}{Max\{Br\} - Min\{Br\}}$$

Define Soil Line Upper – Lower boundaries

$$y_{upper} = mx + b + 0.09$$

Define the wet–water Line

$$Gr(y) = m_1 Br(x) + b_1 - 1.15$$

Define Vegetation–soil and Dense vegetation Lines
(Parallel to Soil Line)

$$Gr(y) = mB_r(x) + b + 0.04$$

$$Gr(y) = mBr(x) + b + 0.09$$

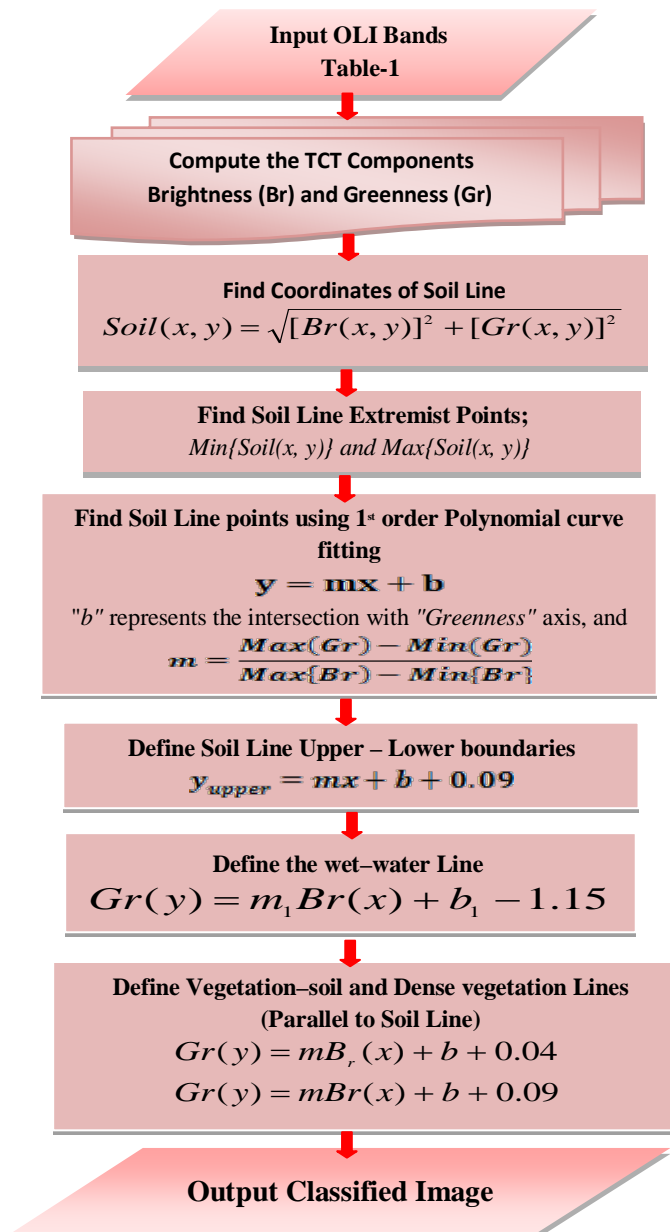**Output Classified Image**

Figure-6: Block-diagram showing the procedures involved in the introduced classification method

In this research, the presented scatterplot classification method is used to predict the vegetated area of OLI bands for the study area; the result is illustrated in Figure-7.
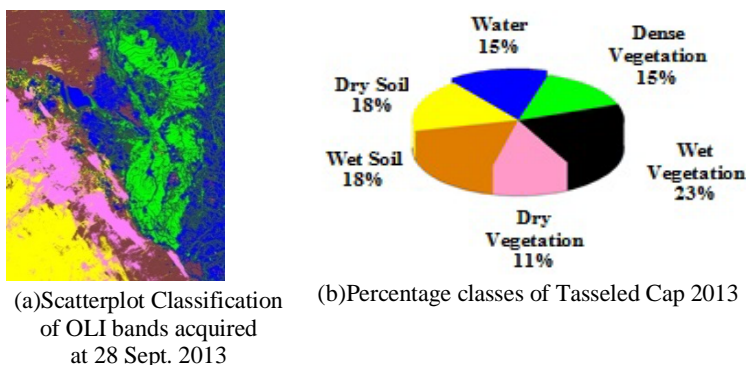

(a)Scatterplot Classification of OLI bands acquired at 28 Sept. 2013

(b)Percentage classes of Tasseled Cap 2013

Figure 7- Illustrates (a) the scatterplot classification of OLI TCT bands, (b) Pie chart showing the percentage of classes.

The dense vegetated areas obtained by implementing the TCT scatterplot classification method is extracted (using the ArcMap package tools) and illustrated in Figure-8.
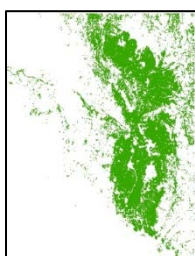
Dense vegetated area 89589.402Hectares,of Landsat-8 OLI bands, at 28 Sept.2013

Figure 8- Extracted dense vegetated area of OLI bands, obtained by implementing the scatterplot of TCT components.

Table-2 shows the accuracy of the calculated acreage by using the TCT classification techniques for the actual acreage, compared with that obtained from the publications of the Iraqi Ministry of Agriculture; i.e. 90577Hectares.

Table 2- Estimation of acreage area by using TCT scatterplot

Data used	Predictive (Agriculture area) Hectares	Accuracy
OLI bands Acquired at 28 Sept. 2013	89589.402	98.91%

The extraction dense vegetative areas of (*Mashkhab)* we have been used Program ArcMap , and their areas were calculated and illustrated in Figure-9 Note: Area = No. of pixels$\times30\times30$ m^2/10000 Hectares.
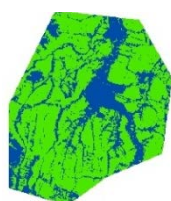
Dense vegetation area 9248.22Hectares, Landsat-8, at September 2013

Figure 9- Extraction region area of study (Mashkhab) depend von Scatter plot (TCT)

Table-3 shows the accuracy of the calculated acreage by using the scatterplot TCT techniques for different way and compared with the actual acreage for the years (2013) that have been obtained from the publications of the Najaf office of Agriculture; i.e. (8750) Hectares for AL-Mashkhab.

Table 3- Estimation Crop of production and its accuracy in AL-Mashkhab

Data Used	Area Hectares	mean production (Kg per Hectares)	Prediction Production (Ton)	Actual Production (Ton)	Accuracy
Landsat 8 (15 Sep.2013)	9248.22	5780.475	**53459.104**	**54625.846**	**97.86%**

Conclusions

The TCT compresses the de-correlated bands of Landsat scenes into fewer bands associated with the physical characteristics of the land surface. Brightness and Greenness bands are the important components mostly used to define the Landcover features. In this paper, a new image classification method is introduced based on the scatterplot behavior of these TCT components. The introduced classification method has adopted our approach followed in our previously published research [8] in determining the soil line and then locating the positions of each class of Landcover components in the scatterplot between the TCT components. The obtained results, as we believe, were satisfactory due to the fact that the data published by the Iraqi Ministry of Agriculture was not accurate.

References

1. Muhammad Hasan Ali Baig, Lifu Zhang, Tong Shuai, and Qingxi Tong. **2014**.Derivation of a tasseled cap transformation based on Landsat 8 at-satellite reflectance, *Remote Sensing Letters,* 5(5), pp:423-431.
2. Kauth R.J. and Thomas G.S. **1976**.The Tasseled Cap –A Graphic Description of the Spectral-temporal development of agricultural crops as seen in Landsat, in Proceedings of the Symposium on Machine Processing of Remotely Sensed Data, University, West Lafayette, Indiana.
3. Malila W.A. and Meyers T.J. **1995**.Tasseled-cap transformation of JERS-1 OPS multispectral data-an initial version, in Geoscience and Remote Sensing Symposium 1.
4. Wang Y. and Sun D.**2005**. The ASTER tasseled cap interactive transformation using Gramm-Schmidt method, in Proceedings of the SPIE, In Zhang L., and others, eds.
5. Eva, lvits, Alistair, L., Filip, L., Scott, H. and Barbara, K.**2008**. Orthogonal Transformation of Segmented SPOT5 Images: Seasonal and Geographical Dependence of the Tasseled Cap Parameters, *Photogrammetric Engineering and Remote Sensing,* 74(11), pp:1351-1364.
6. Horne, J. H.**2003**.A Tasseled Cap Transformation for IKONOS Images, in ASPRS Annual Conference Proceedings, Anchorage, AK, Bethesda, MD: American Society of Photogrammetry and Remote Sensing.
7. Yarbrough L. D., Easson G. and Kuszmaul J. S. **2005**.QuickBird 2 Tasseled Cap Transform Coefficients: A Comparison of Derivation Methods, *Global Priorities in Land Remote Sensing,* 16, pp:23-27.
8. Ali, S.M. **2013**.New Fully Automatic Multispectral Image Classification based on Scatterplot Method, *International Journal of Emerging Technology and Advanced. Engineering,*3(10), pp:388-394.
9. Ali S.M. and Salema S.S. **2016**. Improving the Estimation of Crop of Rice Using Higher Resolution Simulated Landsat Images, *IOSR Journal of Applied Physics (IOSR-JAP),* 8(1), pp: 38-46.